The Investigation of the Synthesis, Characterization, Molecular Docking, and Pharmacokinetic Properties of New Thiocarbohydrazones Based on Schiff Bases

Nalan Turkoz Karakullukcu *

Posted Date: 8 May 2024

doi: 10.20944/preprints202405.0380.v1

Keywords: thiocarbohydrazones; Schiff base; moleculer docking; urease inhibition; pharmacokinetic properties;drug combinations

Article

The Investigation of the Synthesis, Characterization, Molecular Docking, and Pharmacokinetic Properties of New Thiocarbohydrazones Based on Schiff Bases

Nalan Turkoz Karakullukcu

Blacksea Advanced Technology Research and Application Center, Ondokuz Mayis University, 55200, Atakum, Samsun, Turkiye; nturkoz@omu.edu.tr; Tel.: +90-535-7928967

Abstract: Ten new Schiff bases, including thiocarbohydrazone derivatives (**1–10**), were synthesized using an efficient, uncomplicated, and environmentally friendly approach using the reaction of alkyl-substituted aldehydes. The thiocarbohydrazones that were obtained were derived from o-phthalaldehyde. The chemical structures of the compounds were identified by the utilization of UV-Vis spectroscopy, Fourier transform infrared (FT-IR), ^{1}H nuclear magnetic resonance (^{1}H NMR), ^{13}C nuclear magnetic resonance (^{13}C NMR), and elemental analysis methods. The thermal stability of thiocarbohydrazones was examined using thermogravimetric analysis (TGA-DSC). Investigations were conducted on urease inhibition tests, pharmacokinetic property research, and molecular docking. The collection of samples with the urease enzyme revealed significant molecular docking findings, with MolDock scores ranging from -153 to -189. The compounds have the potential to be effective drug candidates for treating certain diseases, as indicated by the consistent results of molecular docking, urease inhibition tests, and pharmacokinetic characteristics investigations.

Keywords: thiocarbohydrazones; Schiff base; moleculer docking; urease inhibition; pharmacokinetic properties;drug combinations

1. Introduction

Schiff bases are chemical compounds characterized by the presence of the imine (>C=N-) functional group. Hugo Schiff first identified these chemicals through the interaction between primary amines and aldehydes, or ketones [1]. Schiff bases are important due to their wide range of applications in biological systems [2], chemical catalysis [3], medicine and pharmacy [4], as well as chemical analysis, and emerging technologies. Schiff bases exhibit many advantageous biological activities and therapeutic effects. The properties of this substance include antibacterial [5], antimicrobial [6], anti-inflammatory [7], antiviral [8], antioxidant [9], anti-HIV [10], cytotoxic [11], antifungal [12], antituberculosis [13], anticancer [14], anthelmintic [15], antiglycation [16], antidepressant [17], and corrosion inhibition [18]. Phthalaldehyde (OPA) has many uses in the field of Schiff base production and investigation [19]. Thiocarbohydrazones are a distinct group of compounds represented by the structural formula =N–NH–C(=S) NH–N= [20]. Thiocarbohydrazones are intriguing ligand systems because of their numerous possible donor sites. Typically, they function as neutral or negatively charged ligands and form a bond with the metal via a sulfur atom and one imine nitrogen atom. This phenomenon arises from the tautomeric equilibrium between the thioketo and thioenol forms. Various variables influence this equilibrium, including the characteristics of the metal ion and its counterion, the circumstances of the reaction, the properties of the solvent, and the pH level of the medium. Extra coordination sites on the lateral substituents may change both the amount of reactants and how well they bind to different metal ions. These traits could be useful in a number of biological contexts, and being able to fine-tune the chelate's stability and properties by changing the coordinating residues of the substituents could have big effects[21,22]. They have diverse applications in the fields of biochemistry [23], pharmaceuticals [24], and industry [25,26].

 doi:10.20944/preprints202405.0380.v1

These compounds exhibit a range of beneficial effects, including their ability to prevent cancer [27,28], DNA repair [28], fight against microbes [29], kill bacteria [24], combat fungal infections [29], act as antioxidants [30], destroy cells [31], inhibit viruses [32], suppress tumor growth [13], and protect against corrosion [33]. Both isatin-based thiocarbohydrazone and Schiff bases possess pharmacological and biological characteristics [34]. Antioxidants have been discovered to confer health advantages by mitigating many types of harm, such as cellular senescence, mutagenic modifications, and the formation of malignant neoplastic tissue. This is accomplished by their capacity to interact with oxygen and nitrogen species, effectively nullifying their radical impacts and therefore mitigating oxidative stress conditions [35]. Antioxidants are molecular substances that disrupt oxidation by limiting the production of free radicals or by controlling the oxidation of biodiesel via the removal of existing radicals [36].These antioxidants have phenolic functional groups in their chemical composition. The antioxidant (AH) acts by impeding the progression of the peroxide radical ($ROO^{\cdot}$) by preventing the production of radicals in the autoxidation pathway [37]. Multiple studies have indicated that Schiff bases exhibit advantageous antioxidant characteristics as a result of the inclusion of a nitrogen atom in the azomethine group, which is located in the sp^2 hybrid orbit. Furthermore, Schiff bases have unshared electron pairs, making them very efficient chelating agents and prone to different reactions [25]. Assessing antioxidant activities is a way to determine the reactivity of Schiff base compounds, which have the capability to create coordination complexes with metal ions. The antioxidative activity of phenolic Schiff bases (SB-OH) is intimately linked to their ability to release hydrogen atoms. There are several ways to scavenge free radicals, which results in the creation of the corresponding phenoxy radical [38,39].

2. Materials and Methods

2.1. Materials

The chemicals and solvents used in this study were procured from reputable suppliers, namely Merck & Co., Inc., located in Kenilworth, NJ, USA, and Sigma-Aldrich Chemical Company, based in St. Louis, MO, USA.

The samples were utilized without undergoing further purification. Thin layer chromatography (TLC) using Kieselgel-60 GF254 (Merck) monitored the progress of the reaction. UV-Vis spectra and absorption data were obtained with a Shimadzu (Shimadzu Corporation, Kyoto, Japan). A Perkin Elmer Spectrum-Two FT-IR spectrometer, manufactured in the USA, was utilized for Fourier transform infrared analysis at ambient temperature. ^{1}H NMR and ^{13}C NMR spectra (in DMSO-d_6) were taken at 25 °C using an Agilent Premium Compact spectrometer operating at 14.1 Tesla and 600 MHz. A Eurovector EA3000 (Eurovector S.r.l., Pavia, Italy) elemental analyzer was used for elemental analysis.

The TGA-DSC analysis was performed using an SDT Q-600 instrument manufactured by TA Instrument-Waters in the USA. The powder samples were subjected to heating at a rate of 10 °C/min in an alumina pan with a nitrogen gas flow rate of 50 mL/min until reaching a temperature of 1100 °C.

A molecular docking study was carried out via the Molegro Virtual Docker 6.0.1. software. Compounds were sketched through Chem-Draw Ultra 18.0, and then Chem3D 18.0 was used to improve energy minimization. The crystal structure of Jack bean urease (4GY7) was obtained from the PDB bank [40]. The binding energy for each molecule with the most suitable binding pose was transferred to the Discovery Studio imaging software to obtain the two-dimensional and three-dimensional shapes [41].

The possible effect of urease inhibition on samples and thiourea at different dosages was evaluated using the spectrophotometric technique. The inhibitory concentration (IC50: µg/mL) was displayed in Table 11. The breakdown of urea produces hypochlorite of ammonia, which nitroprusside interacts with to produce urease inhibitory activity, which was detected at 630 nm [42].

For pharmacokinetic properties, we may more effectively produce highly efficient medical structures and enhance their chemistry and biological uses by assessing their ADME and drug-

 doi:10.20944/preprints202405.0380.v1

likeness properties and estimating their biological activity scores. Every molecule was examined for its MW, TPSA, n-ON acceptor, and n-OHNH donor compliance. Its skin accessibility (Log Kp), blood-brain barrier permeability, soluble rate, and capacity for being taken by human gastrointestinal tissues. SwissADME (http://www.swissadme.ch/index.php) and Molsoft (https://molsoft.com) websites were used in the analyses [43].

2.2. Methods

2.2.1. Synthesis of Schiff Base-Based New Thiocarbohydrazones (**1-10**)

(MA = 134.13 g/mol) o-Phthalaldehyde (1,2-benzenedicarbaldehyde) (5.0 mmol) reacts with thiocarbohydrazide (5.0 mmol) (MA: 106.15 g/mol). Hydrochloric acid, acting as a catalyst, modifies the mixture and dissolves it in 100% ethyl alcohol (20 mL). It is then heated under reflux and agitated. Thin layer chromatography (TLC) is employed to track the progress of the reaction using an executive phase consisting of a mixture of n-hexane and ethyl acetate at a ratio of 4:1. The resulting product is subjected to filtration prior to cooling, followed by numerous washes with cold absolute ethyl alcohol. Subsequently, it is subjected to vacuum drying, and its structure is elucidated. The o-phthalaldehyde-derived thiocarbohydrazone (2.0 mmol) reacts with aldehyde derivatives containing different R groups (2.0 mmol). Each combination is individually modified with HCl (catalyst) and dissolved in 100% ethyl alcohol (25 mL). Next, we heat each combination separately under reflux before mixing them. Thin layer chromatography (TLC) is employed to observe the progression of the processes using an executive phase consisting of a mixture of n-hexane and ethyl acetate at a ratio of 4:1. Once the temperature has decreased in the surrounding environment, the resulting substances from the reaction are separated by filtration. They are then subjected to numerous washes using ethyl alcohol that is 100% pure. After that, the substances are dried under vacuum conditions, and their structure is determined [44,45]. The products exhibited significant yields ranging from 55% to 87% (Figure 1).

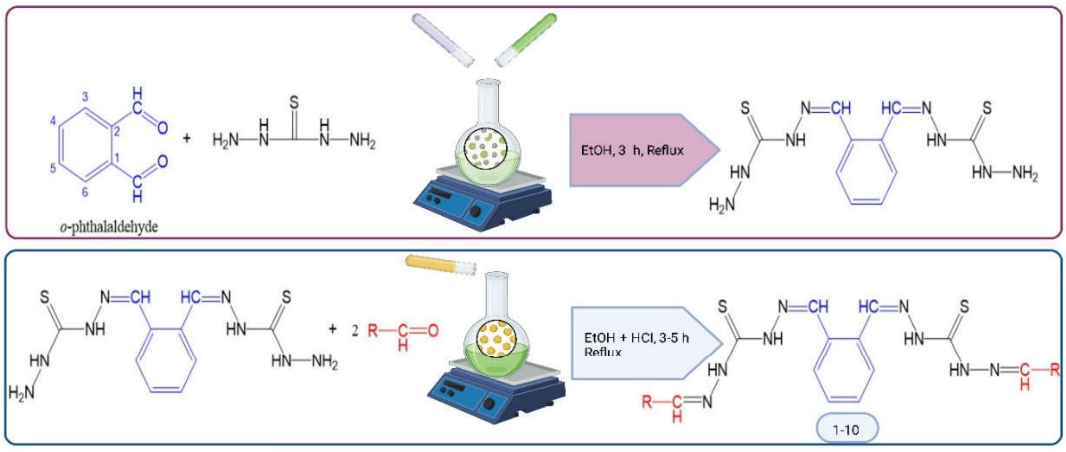

Compound	R	Compound	R
1	C_6H_5	6	3-OCH_3-4-OH-C_6H_3
2	2-OH-C_6H_4	7	3-OH-4-OCH_3-C_6H_3
3	4-OH-C_6H_4	8	2-OH-3-OCH_3-C_6H_3
4	1-naphtyl	9	3-OC_2H_5-4-OH-C_6H_3
5	2,4-diOH-C_6H_3	10	3,5-diOCH_3-4-OH-C_6H_2

Figure 1. The structures and synthesis route for the synthesized new thiocarbohydrazones (**1-10**).

 doi:10.20944/preprints202405.0380.v1

3. Results and Discussion

3.1. Physical Properties

Here are the results for the physical properties, yields, melting points, colors, and elemental analyses (Tables 1 and 2).

Table 1. Physical properties, yields, melting points, and colors all of the synthesized compounds.

Comp.	Compound Name	-R	Yield %	Melting Point (°C)	Color	Color Code [46]
1	N',N'''-(1,2-phenylenebis(methaneylylidene))bis(N'-benzylidenemethanebis(thiohydrazide))	C_6H_5	80	205.26	Brown	$S_{70}O_{26}G_{02}$
2	N',N'''-(1,2-phenylenebis(methaneylylidene))bis(N'-(2-hydroxybenzylidene)methanebis(thiohydrazide))	2-OH-C_6H_4	84	214.01	Dark Brown	$S_{80}O_{07}G_{15}$
3	N',N'''-(1,2-phenylenebis(methaneylylidene))bis(N'-(4-ydroxybenzylidene)methanebis(thiohydrazide))	4-OH-C_6H_4	55	241.44	Black	$S_{99}O_{11}G_{33}$
4	N',N'''-(1,2-phenylenebis(methaneylylidene))bis(N'-(naphthalen-1-ylmethylene)methanebis(thiohydrazide))	$C_{11}H_{10}$	61	232.96	Dark Black	$S_{99}O_{00}G_{02}$
5	N',N'''-(1,2-phenylenebis(methaneylylidene))bis(N'-(2,4-dihydroxybenzylidene)methanebis(thiohydrazide))	2,4-diOH-C_6H_3	77	261.42	Brown	$S_{90}O_{60}G_{11}$
6	N',N'''-(1,2-phenylenebis(methaneylylidene))bis(N'-(4-hydroxy-3-methoxybenzylidene)methanebis(thiohydrazide))	3-OCH_3-4-OH-C_6H_3	81	239.74	Brown	$S_{90}O_{02}G_{50}$
7	N',N'''-(1,2-phenylenebis(methaneylylidene))bis(N'-(3-hydroxy-4-methoxybenzylidene)methanebis(thiohydrazide))	3-OH-4OCH_3-C_6H_3	73	231.96	Brown	$S_{90}O_{11}G_{20}$
8	N',N'''-(1,2-phenylenebis(methaneylylidene))bis(N'-(2-hydroxy-3-methoxybenzylidene)methanebis(thiohydrazide))	2-OH-3OCH_3-C_6H_3	87	298.97	Light Brown	$S_{70}O_{26}G_{33}$
9	N',N'''-(1,2-phenylenebis(methaneylylidene))bis(N'-(3-ethoxy-4-hydroxybenzylidene)methanebis(thiohydrazide))	3-OC_2H_5-4-OH-C_6H_3	78	212.59	Brown	$S_{80}O_{33}G_{33}$
10	N',N'''-(1,2-phenylenebis(methaneylylidene))bis(N'-(4-hydroxy-3,5-dimethoxybenzylidene)methanebis(thiohydrazide))	3,5-diOCH_3-4-OH-C_6H_2	62	295.93	Pale Black	$S_{90}O_{07}G_{41}$

 doi:10.20944/preprints202405.0380.v1

Table 2. Elemental analysis results in all of the synthesized compounds.

Comp.	Molecular mass (g/mol)	Molecular formula	Calculated					Experimental				
			(C)%	(H)%	(N)%	(S)%	(O)%	(C)%	(H)%	(N)%	(S)%	(O)%
1	486.62	$C_{24}H_{22}N_8S_2$	59.24	4.56	23.03	13.18	-	59.30	4.52	23.06	13.12	-
2	518.61	$C_{24}H_{22}N_8O_2S_2$	55.58	4.28	21.61	12.36	6.17	55.57	4.29	21.63	12.37	6.14
3	518.61	$C_{24}H_{22}N_8O_2S_2$	55.58	4.28	21.61	12.36	6.17	55.60	4.28	21.58	12.37	6.17
4	586.74	$C_{32}H_{26}N_8S_2$	65.51	4.47	19.10	10.93	-	65.53	4.45	19.11	10.91	-
5	550.61	$C_{24}H_{22}N_8O_4S_2$	52.35	4.03	20.35	11.65	11.62	52.33	4.04	20.37	11.64	11.62
6	578.67	$C_{26}H_{26}N_8O_4S_2$	53.97	4.53	19.36	11.08	11.06	53.97	4.54	19.35	11.08	11.06
7	578.67	$C_{26}H_{26}N_8O_4S_2$	53.97	4.53	19.36	11.08	11.06	53.96	4.53	19.34	11.09	11.08
8	578.67	$C_{26}H_{26}N_8O_4S_2$	53.97	4.53	19.36	11.08	11.06	53.97	4.54	19.33	11.09	11.07
9	606.72	$C_{28}H_{30}N_8O_4S_2$	55.43	4.98	18.47	10.57	10.55	55.40	4.99	18.50	10.56	10.55
10	638.72	$C_{28}H_{30}N_8O_6S_2$	52.65	4.73	17.54	10.04	15.03	52.65	4.72	17.57	10.05	15.01

3.2. Vibration Frequency Ranges

The vibrations of the substances as measured by FT-IR (Table 3). Presenting the spectral areas associated with certain chemical vibrations generated by the samples. The stretching vibration of the aldehyde group (–CHO) in the first component did not exhibit two bands at 2830–2680 cm^{-1}. The symmetric and asymmetric stretching vibrations of the amino group ($–NH_2$) were not detected in the spectral range of 3400–3150 cm^{-1}. Instead, we detected new stretching vibrations of the imine group around 1570–1481 cm^{-1}. The presence of these peaks serves as an initial indication of the effective synthesis of the materials. The stretching vibrations of ν(O–H) were recorded at a range of 3685–3678 cm^{-1} for all compounds (**1–10**). The stretching vibrations of ν(–C–O) originating from the methoxy and hydroxy groups were observed in the range of 1077–1065 cm^{-1}. The vibrations of the ν(–NH) group in the thiocarbohydrazone area were detected within the range of 3272–3201 cm^{-1}. The ν(-C=S) signals of the thiocarbohydrazone region were seen at 1512–1405 cm^{-1}. The absorptions of the ν(–C–N) group were observed at 1199–1100 cm^{-1}.

Table 3. Experimental FT-IR values for all of the synthesized compounds (cm^{-1}).

Comp.	ν(OH)	ν(NH)	Ar. CH	Aliph. CH	ν(C=N)	ν(NH-C=S)	ν(C-N)	Spec. vib.
1	-	3216	3080	2991	1492	1451	1120	-
2	3679	3201	2991	2929	1491	1464	1191	C-O:1069
3	3680	3207	2990	2921	1514	1456	1166	C-O:1068
4	-	3272	2997	2919	1570	1512	1166	-
5	3685	3254	2990	2911	1509	1411	1100	-
6	3679	3221	2984	2904	1513	1461	1190	C-O:1065
7	3679	3219	2990	2905	1512	1409	1195	C-O:1068
8	3679	3232	2984	2911	1481	1405	1185	C-O:1076
9	3678	3218	2990	2905	1512	1444	1195	C-O:1068
10	3679	3234	2990	2904	1512	1465	1199	C-O:1077

Compound **4** displayed FT-IR emissions that corresponded to distinct functional groupings. The –NH stretching vibration was detected at 3272 cm^{-1}. The existence of this functional group is indicated by the appearance of the –C=N stretching vibration at 1570 cm^{-1}. Furthermore, the presence of the C=S signal in the thiocarbohydrazone area was detected at a frequency of 1512 cm^{-1}. The existence of the C–N bond was shown by the detection of the stretching vibration at 1166 cm^{-1} (Figure 2). The frequency statistics for all molecules were in accordance with the published values for similar compounds [4,47–49].

 doi:10.20944/preprints202405.0380.v1

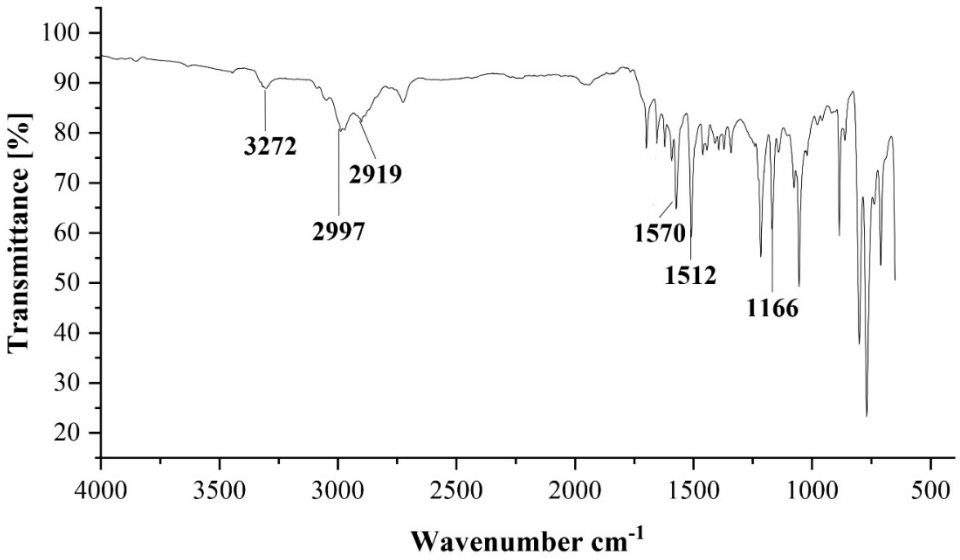

Figure 2. FT-IR spectrum of synthesized compound **4**.

3.3. The Interpretation of the ^1H Nuclear Magnetic Resonance Spectrum

The NMR spectra of all compounds using deuterated dimethyl sulfoxide (DMSO-d_6) as the solvent. They found that DMSO-d_6 and water exist in DMSO (HOD, H_2O) at chemical shifts of about 2.00, 2.55 (quintet), and 3.40 ppm (variable, depending on the solvent and its concentration).

Shows the chemical shifts for all compounds, excluding compound **4** (Table 4). The proton signals attributed to the imine (-CH=N) groups in compounds **1–10** were seen as singular peaks within the chemical shift ranges of 8.58–8.52 ppm. The singlet signals of the amino groups (-N_2H and -N_1H) inside the thiocarbohydrazone moiety were seen at chemical shift ranges of 11.62–10.63 and 10.66–9.74 ppm, respectively. The proton signals for the hydroxyl groups (-OH) in compounds **1–10** were seen as singlets, with chemical shifts ranging from 13.46 to 8.75 ppm. For compounds **6**, **7**, **8**, and **10**, the proton signals of the methoxy group (-OCH_3) showed a singlet at 3.79, 3.80, 3.80, and 3.83 ppm, respectively.

The H1, H3, and H4 protons showed doublet peaks at 8.01–7.88 ppm, 7.66–7.64 ppm, and 8.35–8.33 ppm, respectively. The H2 proton is coupled to the H1 and H3 protons, and the observed doublet of doublets peakes at 7.55–7.54 (J = 7.5, 1.8 Hz) ppm. The H5 proton was coupled to the H4 and H6 protons and showed triplet peaks at 7.54–7.53 (J = 8.0 Hz) ppm. The H6 proton was coupled to the H5 and H7 protons and showed a doublet of doublet peaks at 7.54–7.53 (J = 8.0, 3.0 Hz) ppm. The H7 proton was detected as a doublet peak at 7.75–7.73 ppm. The H8 proton was detected as a doublet peak at 7.60–7.57 ppm. The H9 proton was coupled to the H8 and H9 protons and showed doublet of doublets peaks at 7.44–7.42 (J = 8.1, 3.0 Hz) ppm. For compound **9**, the proton signal of the methylene group (-CH_2) was observed as a doublet of doublets peaking at 4.07–4.03 (2H, dd, J = 6.2 Hz) ppm; the methyl group (-CH_3) was detected as a triplet at 1.33–1.31 (1H, t, J = 6.2 Hz) ppm.

 doi:10.20944/preprints202405.0380.v1

Table 4. ^{1}H NMR (δ, ppm, in DMSO- d_6) values of synthesized compounds except **4**.

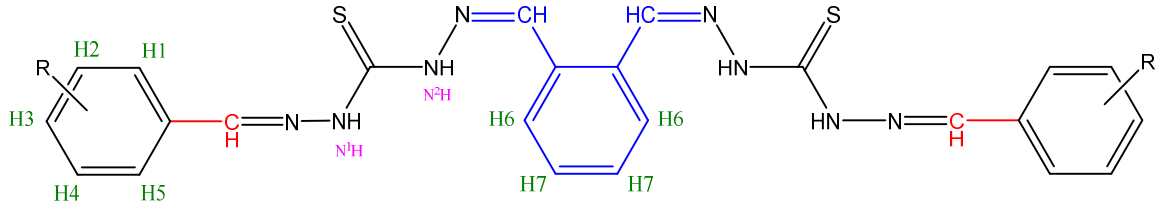

1-3 and 5-10

Comp.	H1	H2	H3	H4	H5	H6	H7	N^1H -N	N^2H-N	CH=N	O-H	Spec. peaks
1	7.74-7.73 d	7.50-7.48 dd	7.45-7.43 dd	7.48-7.46 dd	7.73–7.72 d	7.66-7.64 d	7.43–7.42 dd	9.83 s	11.62 s	8.58 s	-	-
2	-	6.95-6.93 d	7.31-7.28 dd	6.93-6.91 dd	7.52-7.50 d	7.66-7.64 d	7.44-7.42 dd	10.64 s	10.64 s	8.56 s	11.04 s	-
3	7.53-7.52 d	6.89-6.88 dd	-	6.87-6.87 dd	7.54-7.54 d	7.66-7.63 d	7.45-7.41 dd	9.83 s	11.50 s	8.56 s	9.69 s	-
5	-	6.56-6.55 s	-	6.55-6.53 d	7.49-7.48 d	7.67-7.63 d	7.45-7.41 dd	10.63 s	10.63 s	8.56 s	11.69 s 10.11 s	-
6	7.25-7.24 s	-	-	6.89-6.87 d	7.27-7.25 d	7.67-7.63 d	7.45-7.41 dd	9.83 s	11.62 s	8.56 s	9.50 s	-OCH_3: 3.79, s
7	7.28 s	-	-	7.05-7.03 d	7.40-7.38 7.20-7.17 m	7.66-7.64 d	7.44-7.42 dd	9.86 s	11.62 s	8.54 s	9.24 s	-OCH_3: 3.80, s
8	-	-	6.99-6.97 d	6.96-6.94 dd	7.16-7.14 dd	7.67-7.63 d	7.45-7.41 dd	10.66 s	10.66 s	8.54 s	13.46 s	-OCH_3: 3.80, s
9	7.25-7.24 s	-	-	6.88-6.86 d	7.27-7.25 d	7.67-7.63 d	7.45-7.41 dd	9.74 s	10.98 s	8.53 s	9.62 s	-CH_2: 4.07-4.03 d d -CH_3: 1.33-1.31 t
10	7.00-6.99 s	-	-	-	7.00-6.99 s	7.67-7.63	7.45-7.41	9.95 s	11.50 s	8.52 s	8.75 s	-OCH_3: 3.83 s

s singlet, d doublet, dd doublet of doublet, dt doublet of triplet, t triplet, td triplet of doublet, m multiplied.

In compound **4**, the signal of imine (-CH=N) was observed as a singlet at 8.55 ppm. The -N^1H and -N^2H proton signals of the thiosemicarbazone region were observed as a singlet at 10.63 ppm. Table 5 displays the chemical shifts of compound **4**. Figure 3 displays the aromatic proton signals of the thiosemicarbazone ring (H1–H7), which were identified within the range of 8.35 to 7.53 ppm (please see supplementary information). These results are highly consistent with values for similar compounds [50–54].

Preprints.org (www.preprints.org) | NOT PEER-REVIEWED | Posted: 8 May 2024 doi:10.20944/preprints202405.0380.v1

Table 5. ^{1}H NMR (δ, ppm, in DMSO-d_6) values of the synthesized compound **4**.

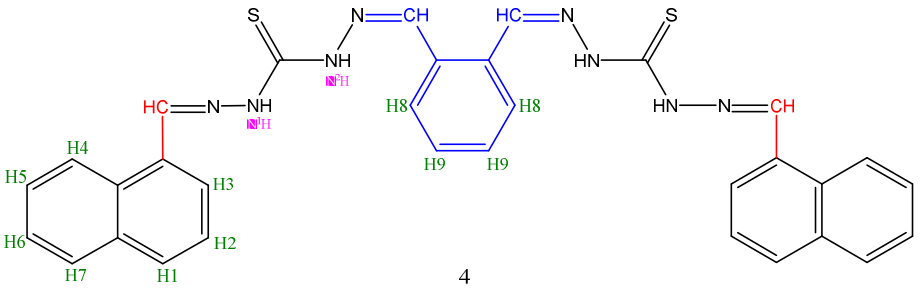

4

Comp.	H1	H2	H3	H4	H5	H6	H7	N^{1}H-N	N^{2}H-N	CH=N	O-H	Spec. peaks	
4	8.01-7.88 d	7.55-7.54 dd	7.66-7.64 d	8.35-8.33 d	7.54-7.53 dd		7.75-7.73 d	10.63 s	10.63 s	8.55 s	-	H8 7.60-7.57 d	H9 7.44-7.42 dd

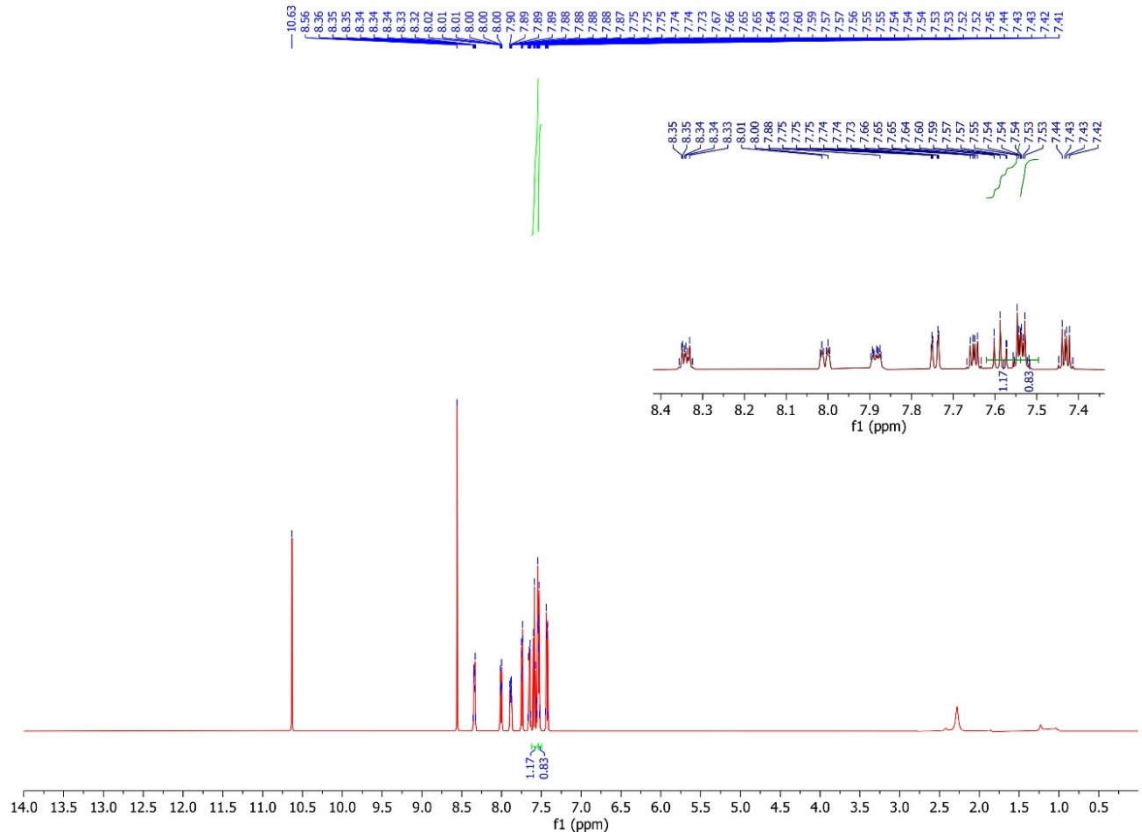

Figure 3. ^{1}H NMR (δ, ppm, in DMSO-d_6) spectrum of synthesized compound **4**.

3.4. The interpretation of the ^{13}C Nuclear Magnetic Resonance Spectrum

The ^{13}C NMR spectra of the compounds were taken in DMSO-d_6; the chemical shifts are summarized in Tables 6 and 7, respectively. In the compounds (**1–9**), the aromatic C signals of the aryl ring (C1–C6) were observed between 163.4 and 111.4 ppm, and those from the terephthalaldehyde ring (C9–C10) were observed between 141.1 and 128.2 ppm.

Preprints.org (www.preprints.org) | NOT PEER-REVIEWED | Posted: 8 May 2024 doi:10.20944/preprints202405.0380.v1

Table 6. ^{13}C NMR (δ, ppm, in DMSO-d_6) values of synthesized compounds except **4**.

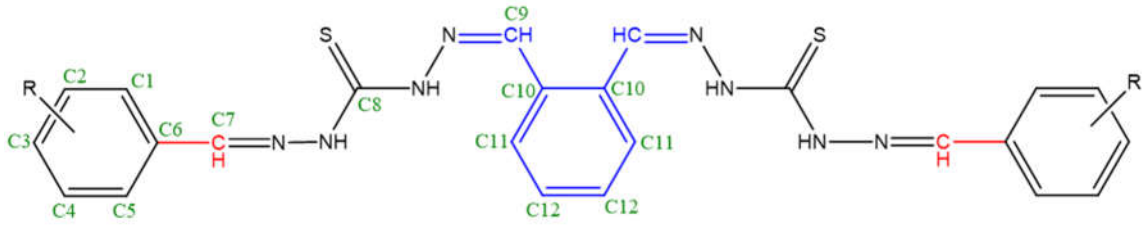

1-3 and 5-10

Comp.	C1	C2	C3	C4	C5	C6	C7	C8	C9	C10	C11	C12	R
1	129.02	128.62	132.01	128.62	129.02	133.51	147.53	184.25	145.64	134.30	129.02	132.01	-
2	158.88	117.99	132.80	121.06	127.84	118.78	147.14	185.75	142.96	136.19	129.02	130.51	-
3	132.43	116.0	160.77	116.0	132.43	125.95	148.32	184.96	142.08	134.69	129.02	133.90	
5	163.12	103.82	162.62	110.03	133.67	111.76	146.24	185.11	144.54	134.14	129.25	131.46	-
6	114.44	149.66	151.55	117.91	122.64	131.93	146.75	185.67	144.30	134.69	129.73	132.49	-OCH_3: 57.64
7	125.08	153.60	155.03	120.35	127.33	131.46	150.50	184.19	145.34	136.11	129.49	131.46	-OCH_3: 56.21
8	155.81	151.39	115.94	118.38	126.26	120.67	148.48	187.64	145.49	137.84	130.75	133.43	-OCH_3: 56.31
9	113.26	148.48	153.60	116.41	123.55	130.99	146.27	186.14	143.30	135.64	129.49	132.96	O-CH_2: 65.75 CH_2-CH_3: 15.15
10	107.35	149.90	140.84	149.90	107.35	128.23	146.98	185.90	143.87	135.87	129.25	131.46	-OCH_3: 56.61

Table 7. ^{13}C NMR (δ, ppm, in DMSO-d_6) values of the synthesized compound **4**.

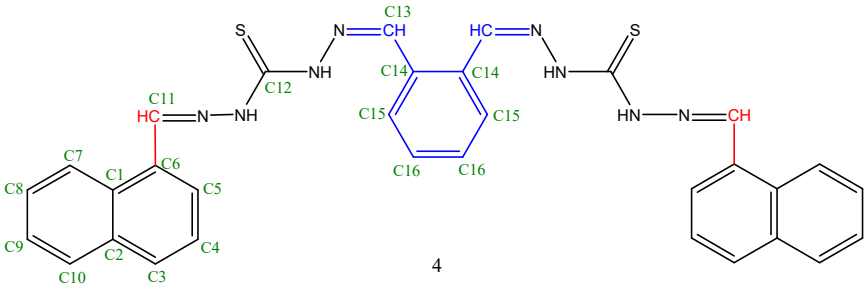

4

Comp.	C1	C2	C3	C4	C5	C6	C7	C8	C9	C10	C11	C12	C13	C14	C15	C16
4	135.61	137.16	131.25	126.59	124.58	133.67	125.71	120.10	127.28	130.18	162.29	194.75	169.17	135.61	127.97	129.38

The imine compounds **1-3** and **5-10** exhibited distinctive peaks at 150.50 and 142.08 ppm, respectively, corresponding to the –C=N (C7 and C9) functional groups. Compounds **1-3** and **5-10**, respectively, exhibited notable –C=S (C8) peaks at 187.64 and 184.19 ppm in the thiosemicarbazone area. The methoxy carbon atoms (–OCH_3) in compounds **6**, **7**, **8**, and **10** exhibited resonance between 57.64 and 56.21 ppm. Compound **9** showed a methylene carbon signal at 65.75 ppm. Please refer to the supplementary material for further details.

Compound **4** exhibited a ^{13}C NMR spectrum with **10** distinct resonances, which aligns with the structure depicted in Figure 4. The thiosemicarbazone part of compound **4** showed a -C=S (C12) signal with a 194.75 ppm chemical shift. The imine compound exhibited a distinctive -C=N (C11 and C13) peak, which was detected at chemical shifts of 162.29 and 169.17 ppm, respectively. The carbon atoms (C1–C10) of the ring containing two aryl groups were identified with chemical shifts of 135.61, 137.16, 131.25, 126.59, 124.58, 133.67, 125.71, 120.10, 127.28, and 130.18 ppm, respectively. The chemical shifts of the aromatic carbon signals in the terephthalaldehyde region (C14–C16) were detected at 135.61, 127.97, and 129.38 ppm, respectively. These results are consistent with the data published for analogous substances [51,55–57].

 doi:10.20944/preprints202405.0380.v1

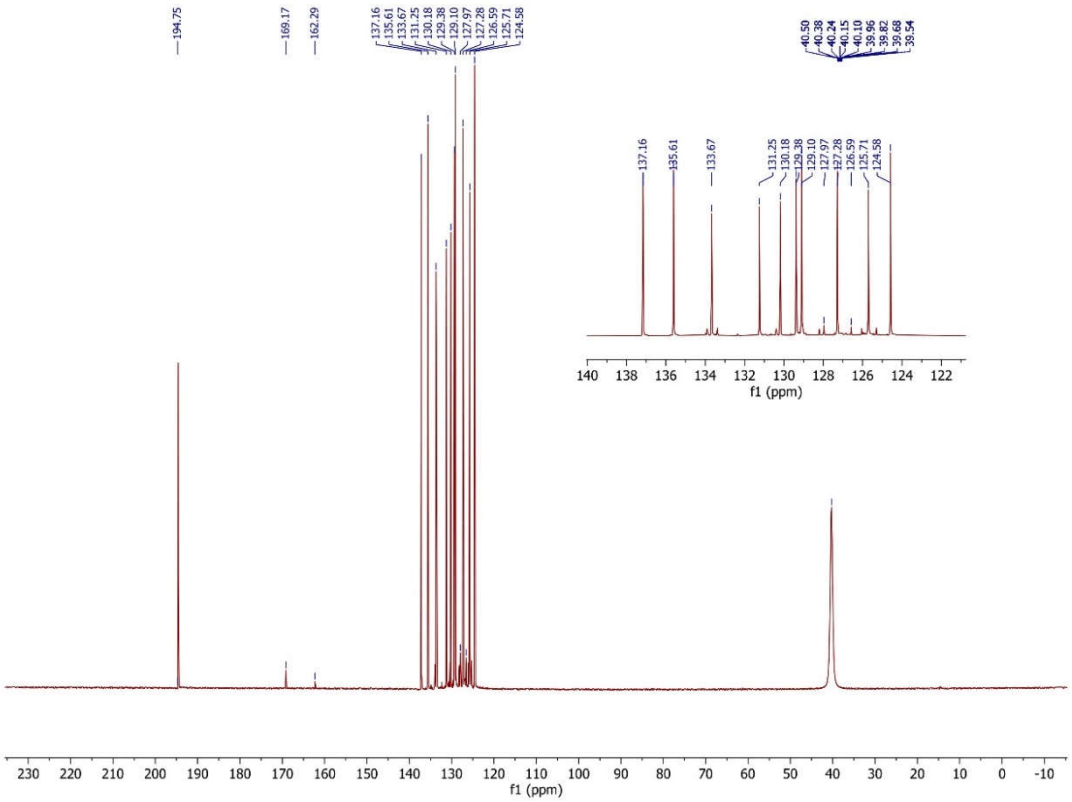

Figure 4. ^{13}C NMR (δ, ppm, in DMSO- d_6) spectrum of synthesized compound **4**.

3.5. Analysis of the UV–Vis Spectra

The electronic absorption spectra of the newly synthesized thiocarbohydrazones, which are derived from Schiff base derivatives (**1–10**), indicate that absorption bands within the wavelength range of 240–350 nm were seen in all the products produced, namely in dimethylsulfoxide. The compounds exhibit notable absorption bands in their electronic spectra, namely in the aromatic ring (C=C) and thiocarbohydrazone (C=S)–imine (CH=N) area. These bands can be attributed to transitions of a π → π * and an n → π *. All compounds exhibit π → π * type transitions of C=C on the aromatic ring within the wavelength range of 240–260 nm. The n → π * transitions of the imine C=N double bond were seen at a wavelength of 280 nm, with the exception of compound **4** which exhibited a transition at 260 nm. The spectral bands seen within the range of 310–350 nm can be attributed to the electronic transition n → π * of the thiocarbohydrazone moiety possessing the C=S group.

The thiocarbohydrazone moiety (C=S) in compound **4** exhibits 2 n → π * transitions at 310 (shoulder) and 340 nm, as seen in Figure 5. The bands observed at 260 nm (shoulder) correspond to the azomethine C=N double bond and the n → π * transitions. On the other hand, the π → π * transitions of C=C on the aromatic structure are observed at 240 nm, as depicted in Figure 5. Table 8 provides a summary of the electronic spectrum data for all the substances. The observed values align with the findings published for analogous substances [2,57,58]. Please refer to the supplementary material for further details.

 doi:10.20944/preprints202405.0380.v1

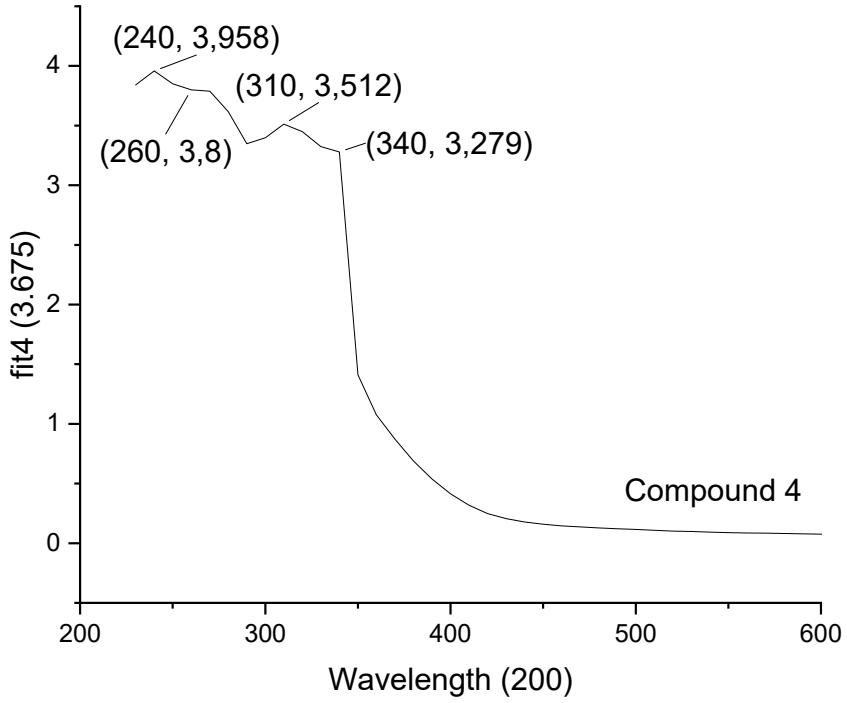

Figure 5. UV–Vis spectrum of compound **4** in DMSO-d_6.

Table 8. Electronic spectral data (nm) of all the synthesized compounds (**1–10**) in DMSO-d_6.

Compound	$\pi \rightarrow \pi^*$, B band	$n \rightarrow \pi^*$, C=N	$n \rightarrow \pi^*$, C=S
1	240	280	330
2	240	280	340
3	240	280	330
4	240	260	310, 340
5	250	280	350
6	260	280	340
7	240	280	340
8	260	280	330
9	250	280	340
10	240	280	320

3.6. Thermal Properties

Thermal properties such as onset temperature (Ton), weight loss% values, and melting point temperature (Tm) values were obtained from TGA-DSC analysis, and these values were calculated from thermal curves. The thermal analysis curve of compound **4** and the calculation results for all of them are shown in Figure 6 and Table 9, respectively. The TGA curve of compound **4** showed a single decomposition step. The step was at a temperature range of 169.43–234.47 °C, and it suited the loss of the thiocarbohydrazone group (94.39%, 8.9 mg). The Tm values of thiocarbohydrazones (**1-10**) were calculated as 205.26, 214.01, 241.44, 232.96, 261.42, 239.74, 231.96, 298.97, 212.59, and 295.93 C, respectively. Ton values of thiocarbohydrazones (**1-10**) were calculated as 195.69, 200.98, 228.08, 169.43, 236.94, 211.38, 217.53, 207.42, 200.22, and 211.37 °C, respectively. It is seen from the TGA curves in Figure 7 that all of the thiocarbohydrazones have a degradation step (between 25 and 1100 °C). The weight loss% values of Schiff bases were found to be 74.20, 58.42, 54.63, 94.39, 54.93, 58.83,

 doi:10.20944/preprints202405.0380.v1

58.02, 63.82, 65.13, and 61.56%, respectively. The TGA results were evaluated according to the literature [59–61]. Please refer to the supplementary material for further details.

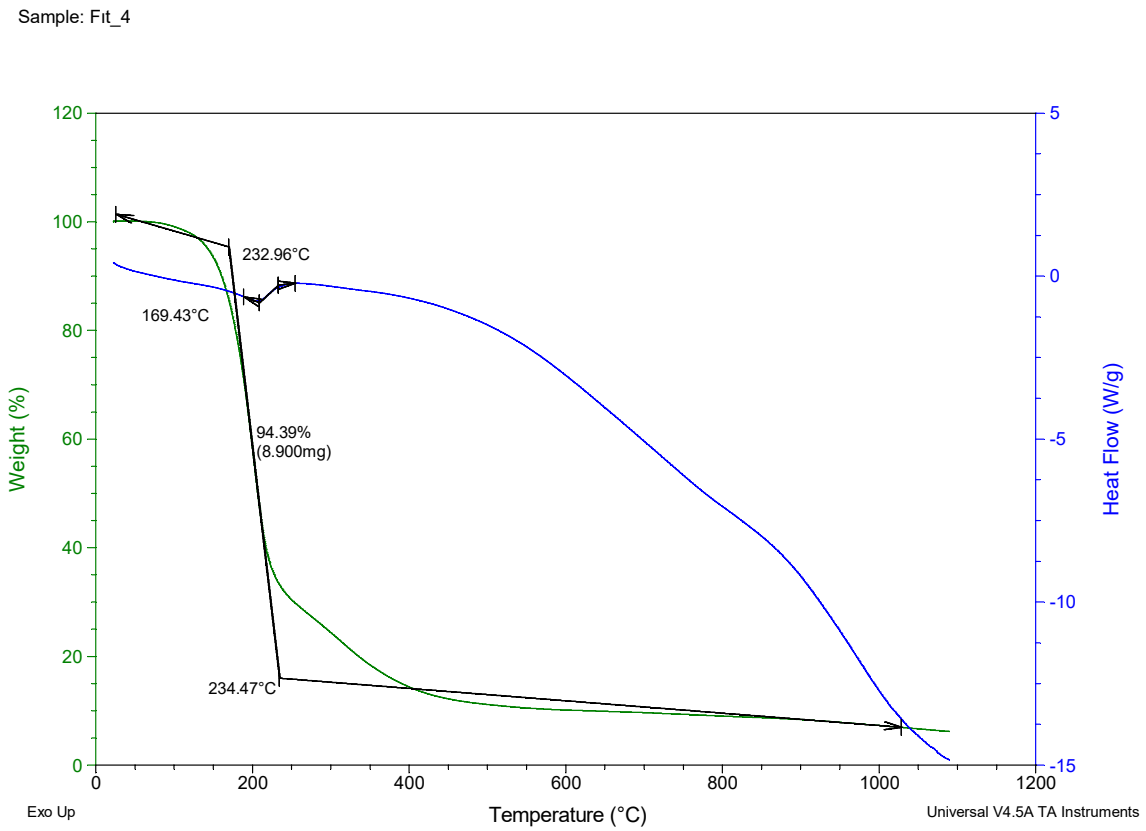

Figure 6. TGA and DSC curves for synthesized compound **4.**

Table 9. Results obtained from the TGA-DSC analyses.

Compounds	TGA	TGA	DSC
	[a]Ton	[b]Weight loss % at 1100 °C	[c]Tm (°C)
1	195.69	74.20	205.26
2	200.98	58.42	214.01
3	228.08	54.63	241.44
4	169.43	94.39	232.96
5	236.94	54.93	261.42
6	211.38	58.83	239.74
7	217.53	58.02	231.96
8	207.42	63.82	298.97
9	200.22	65.13	212.59
10	211.37	61.56	295.93

a: The onset temperature. **b:** Weight loss %. **c:** Melting point temperature.

 doi:10.20944/preprints202405.0380.v1

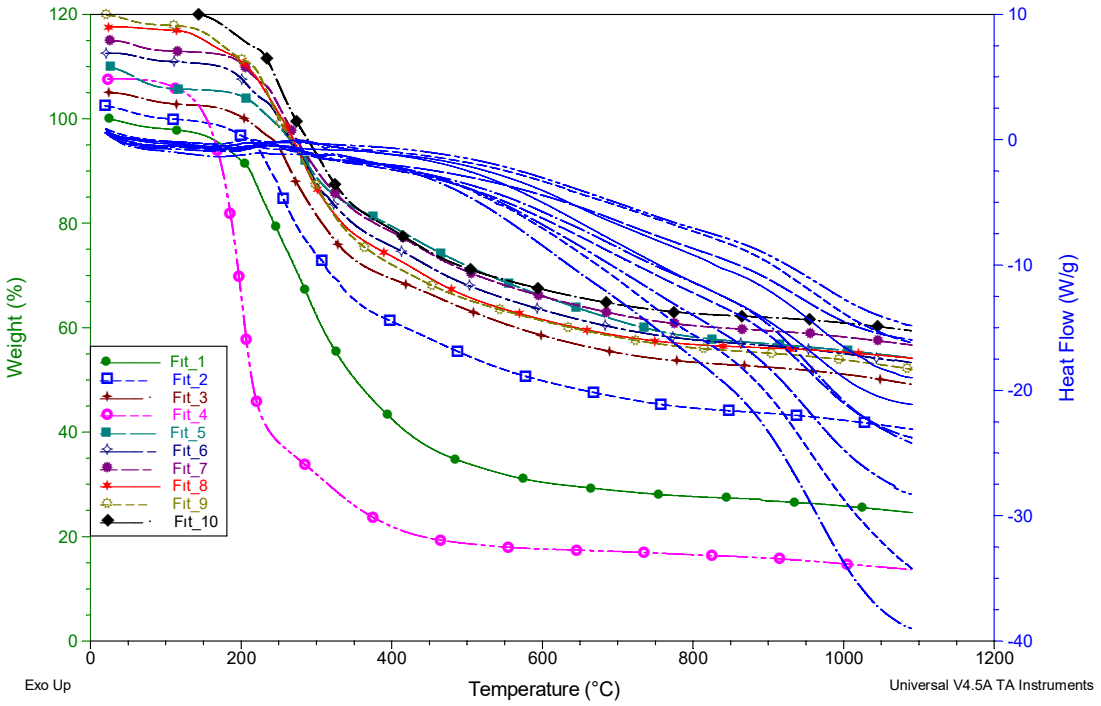

Figure 7. Thermogravimetric analyses (TGA-DSC) of the synthesized compounds.

3.7. Molecular Docking and Urease Inhibition

Urease is a crucial enzyme in the metabolic system that is related to the hydrolysis of urea. It is critical to discover compounds that can control this enzyme's activity. In general, the series of samples gave high molecular docking results with the urease enzyme between -153 to -189 MolDock scores. This indicates that the interaction between these compounds and the protein proceeds smoothly. However, the highest value was recorded by compound **4** with a MolDock score of -189.

Table 10. Moldock scores and inhibition activity values (IC50: μg/mL) for the samples with the urease.

Comp.	1	2	3	4	5	6	7	8	9	10	thiourea
MolDock Score	-160	-171	-175	-189	-161	-177	-170	-153	-175	-186	-
IC_{50} (μg/mL)	88.11±1.95	39.00±1.17	39.86±1.04	20.79±0.68	39.89±0.40	31.28±0.00	45.78±0.40	84.97±1.07	38.01±0.37	27.11±0.00	37.13±1.38

As for the nature of the interactions, they were as follows: the interaction of the first compound **1** with urease was produced through nine bonds as: two conventional H-bonds with GLY641 and GLU642 residues, C-H bonds with THR715, two pi-donor H-bonds with VAL640 and SER645 residues, four pi-alkyl hydrophobic interactions with ARG639, VAL640, LYS716 and MET746 residues Figure 8.

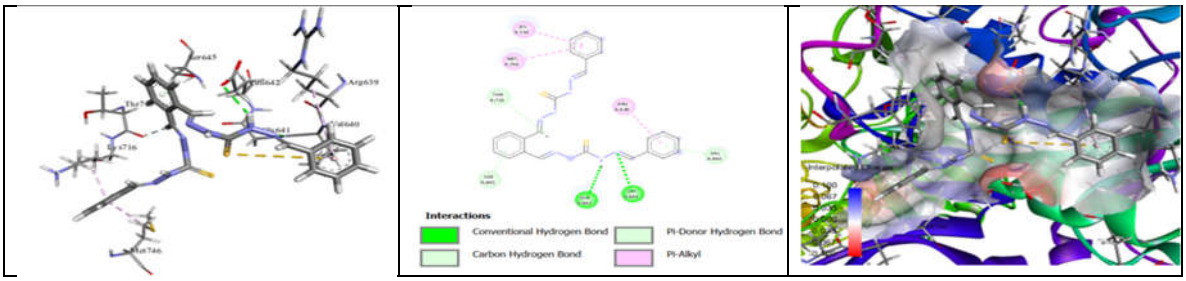

Figure 8. Molecular docking scheme for the compound **1**-urease complex.

 doi:10.20944/preprints202405.0380.v1

The interaction between compound **2** and urease was produced through nineteen bonds as follow; seven conventional H-bonds with VAL640, GLU642, SER421, SER421, GLY638, PRO717 and ASP730 residues, two C-H bonds with SER634 and SER421 residues, a pi-cation electrostatic interaction with LYS716, pi-anion electrostatic interaction with GLU418 residue, two pi-sulfur interactions with CYS412 and PHE838 residues, pi-pi T-shaped hydrophobic interaction with PHE838 residue, four pi-alkyl hydrophobic interactions with LEU415, VAL640, LYS716 and MET746 residues Figure 9.

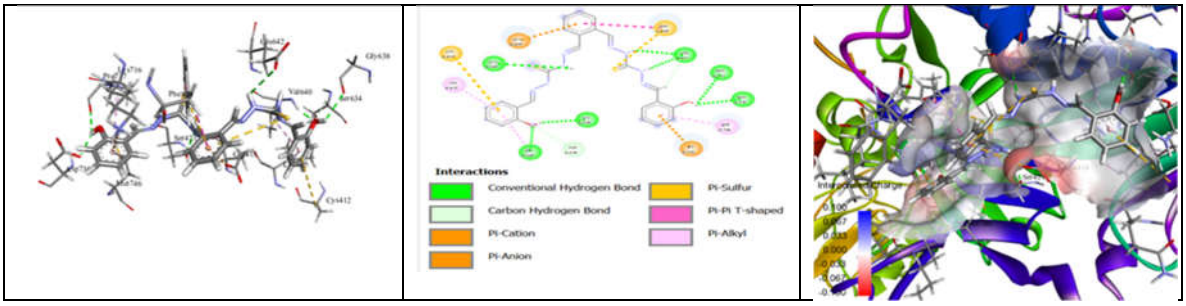

Figure 9. Molecular docking scheme for the compound **2**-urease complex.

The interaction between compound **3** and urease formed via eleven interactions as follow; conventional H-bond with ASP730 residue, two C-H bonds with MET637 and SER421 residues, pi-anion electrostatic interaction with GLU642 residue, two pi-sulfur interactions with MET588 and PHE838 residues, amide-pi stacked hydrophobic interaction with MET637:C, O; GLY638: N residues, four pi-alkyl hydrophobic interactions with ARG639, ARG639, LYS716 and MET746 residues Figure 10.

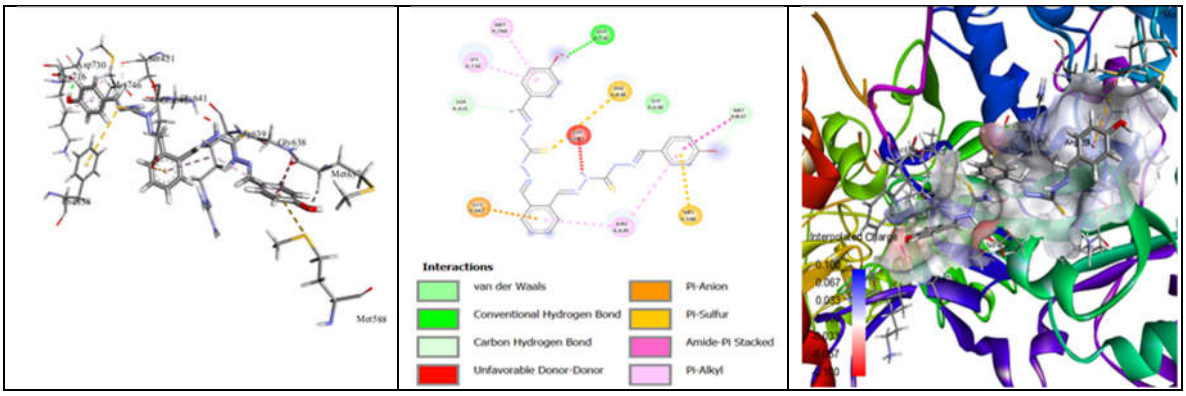

Figure 10. Molecular docking scheme for the compound **3**-urease complex.

Compound **4** has interacted with urease within sixteen bonds as follows; four conventional H-bonds with GLY641, GLU418, SER421, and SER421 residues, C-H bond with GLY641 residue, pi-cation electrostatic interaction with GLY641 residue, two pi-anion electrostatic interactions with ASP730 and ASP730 residues, two pi-sulfur interactions with CYS412 residue, pi-pi stacked hydrophobic interaction with PHE712 residue, five pi-alkyl hydrophobic interactions with LEU415, VAL640, LYS716 and LEU415 residues Figure 11.

Preprints.org (www.preprints.org) | NOT PEER-REVIEWED | Posted: 8 May 2024 doi:10.20944/preprints202405.0380.v1

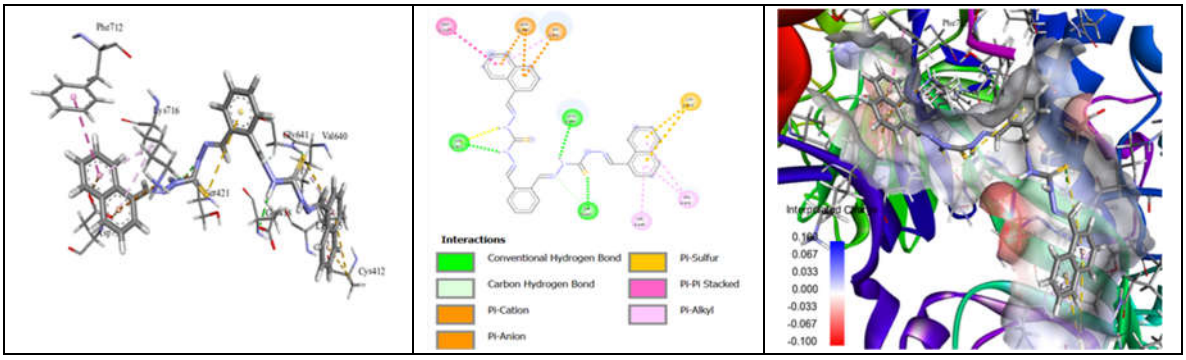

Figure 11. Molecular docking scheme for the compound **4**-urease complex.

The interaction between compound **5** and urease via thirteen bonds as follows; four conventional H-bonds with MET746, SER421, SER421 and THR715 residues, two C-H bonds with MET746 and GLY641 residues, two pi-cation electrostatic interactions with LYS716 and ARG747 residues, pi-anion electrostatic interaction with ASP730 residue, pi-sigma interaction with LYS716 residue, three pi-alkyl hydrophobic interactions with MET746, LYS745 and ARG747 residues Figure 12.

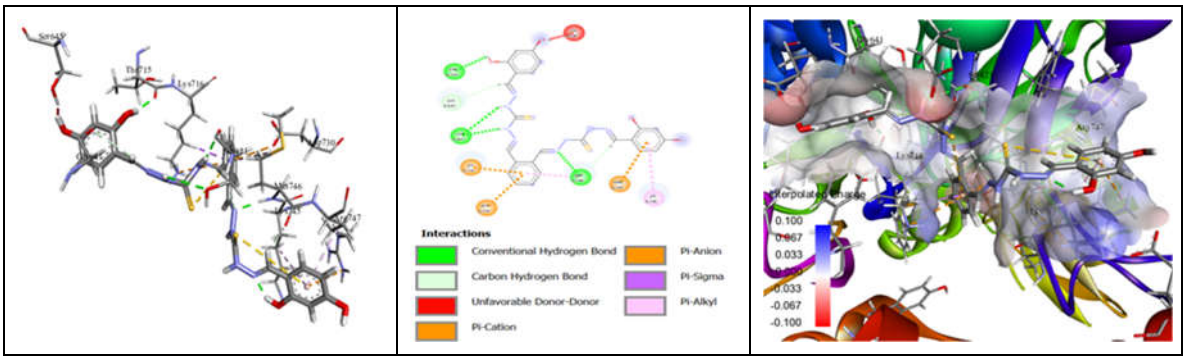

Figure 12. Molecular docking scheme for the compound **5**-urease complex.

The interaction between compound **6** and urease via thirteen bonds as follows; two conventional H-bonds with SER421 and GLU418 residues, five C-H bonds with THR715, VAL744, GLY714, GLY641 and THR715 residues, pi-cation electrostatic interaction with LYS716 residue, two pi-anion electrostatic interactions with GLU418 and ASP730 residues, pi-sigma hydrophobic interaction with LYS716 residue, pi-lone pair interaction GLY641 residue, alkyl hydrophobic interaction with ILE644 residue Figure 13.

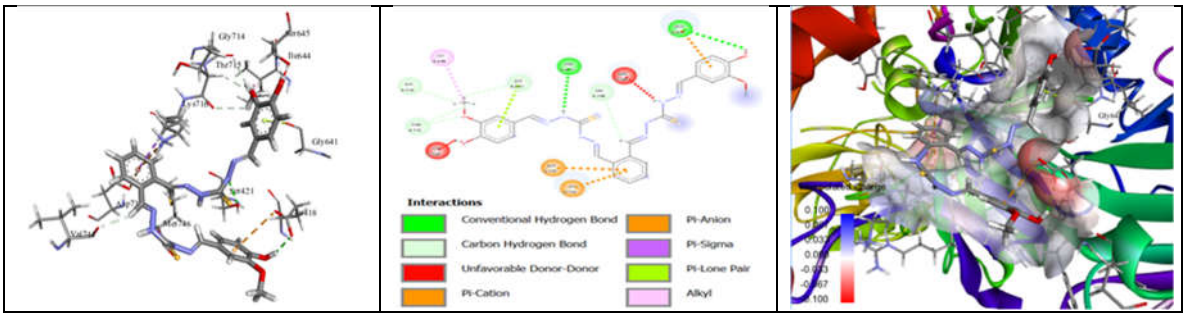

Figure 13. Molecular docking scheme for the compound **6**-urease complex.

Compound **7** has interacted with urease within fourteen bonds as follows; attractive charge (salt bridge) electrostatic interaction with GLU418 residue, attractive charge electrostatic interaction with GLU642 residue, two conventional H-bonds with GLU642 residue, two C-H bonds with GLY642 and ASP730 residues, pi-anion electrostatic interaction with PHE840 residue, pi-donor H-bond with

 doi:10.20944/preprints202405.0380.v1

GLY641 residue, two alkyl interactions with LYS716 and LEU839 residues, four pi-alkyl hydrophobic interactions with ARG639, VAL640, LYS716 and MET746 residues Figure 14.

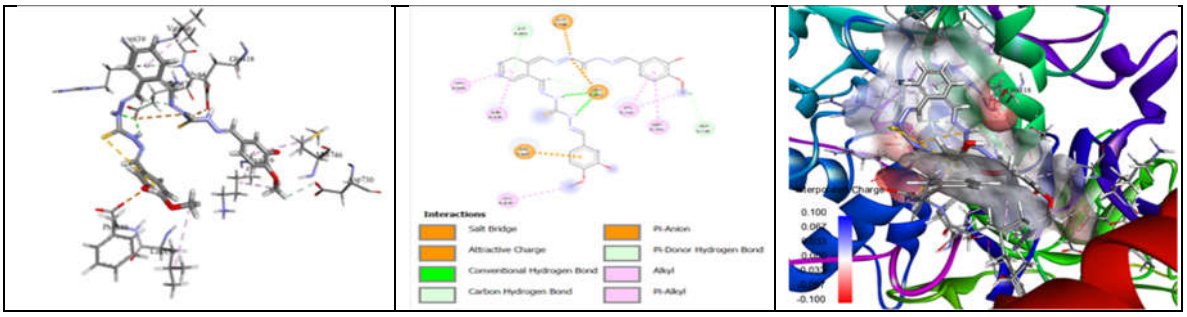

Figure 14. Molecular docking scheme for the compound **7**-urease complex.

The interaction between compound **8** and urease was created through twelve interactions as follows; four conventional H-bonds with MET746, SER421, THR715, and GLU418 residues, C-H bond with GLU642 residue, pi-cation electrostatic interaction with LYS716 residue, pi-anion electrostatic interaction with GLU418 residue, pi-donor H-bond with MET746 residue, pi-sigma hydrophobic interaction with LYS746 residue, pi-pi T-shaped interaction with PHE838 residue, two pi-alkyl hydrophobic interaction with PHE838 residue Figure 15.

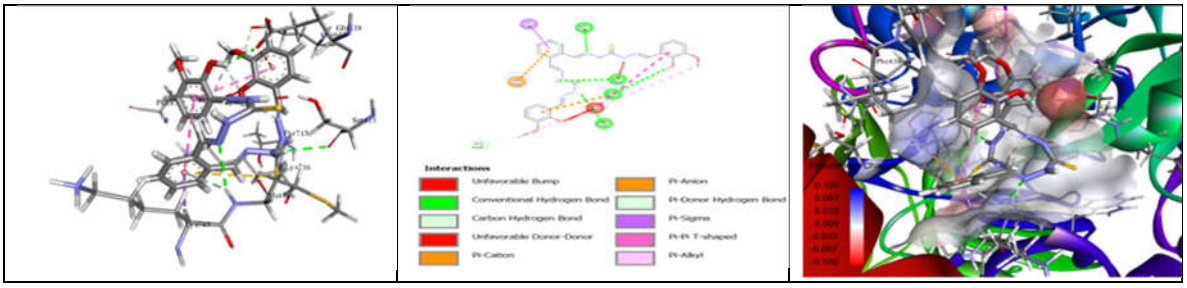

Figure 15. Molecular docking scheme for the compound **8**-urease complex.

The interaction between compound **9** and urease was generated through eleven interactions as follows; three conventional H-bonds with GLU418, GLU418, and PRO717 residues, pi-pi T-shaped hydrophobic interaction with TRP728 residue, three alkyl hydrophobic interactions with LYS716, MET746 and PRO748 residues, four pi-alkyl hydrophobic interactions with TRP728, LYS716, PRO717 and MET746 residues Figure 16.

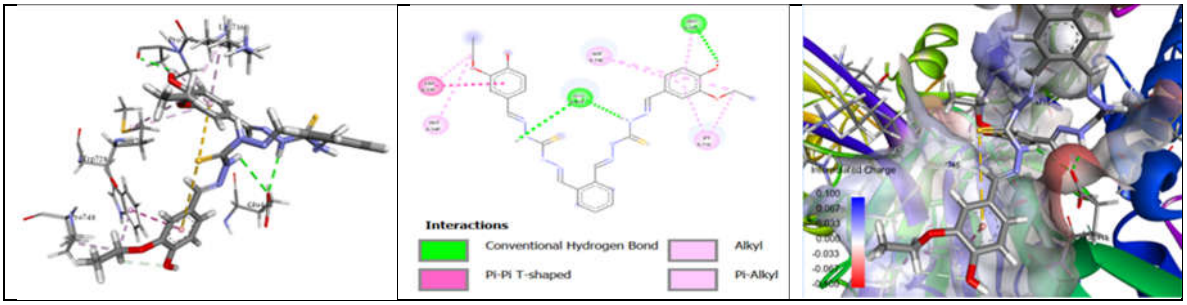

Figure 16. Molecular docking scheme for the compound **9**-urease complex.

The interaction between compound **10** and urease was created via seventeen interactions as follows; three conventional H-bonds with SER645, ARG835, and GLY641 residues, six C-H bonds with SER834, GLY641, SER834, PHE840, PRO717 and ASP730 residues, pi-anion electrostatic interaction with PHE840 residue, pi-pi stacked electrostatic interaction with PHE838 residue, two

 doi:10.20944/preprints202405.0380.v1

alkyl hydrophobic interactions with LYS716 and MET746 residues, four pi-alkyl hydrophobic interactions with PHE838, ARG835, LYS716 and MET746 residues Figure 17.

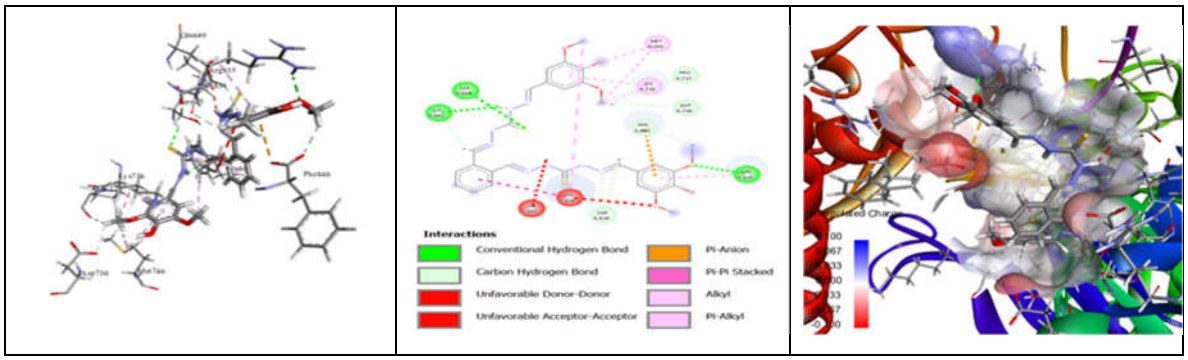

Figure 17. Molecular docking scheme for the compound **10**-urease complex.

3.8. Pharmacokinetic Properties

Since the enzyme urease occupies a location in the human digestive system, it is natural for us to test whether our compounds have the ability to reach the digestive system and how the substances will behave within the system. Compounds were examined for adherence to MW, TPSA, n-ON receptor, and n-OHNH donors. Furthermore, the permeability level (Log Kp) in both the epidermis layer and the blood-brain barrier, as well as the solubility and absorption capacity in human gastrointestinal cells, have been evaluated for each of them (Table 11). However, our results show that the properties of all compounds were investigated in terms of MW, TPSA, H-bonds acceptors, and donors' conformance. In addition, blood-brain barrier permeability, solubility, and the ability to be absorbed by human intestinal cells. In general, our results provide information about the synthesized molecules' absorption, distribution, metabolism and excretion. The majority of the compounds with acquired ADME parameters were found to be within acceptable boundaries and did not vary from Lipinski's rules.

Table 11. Basic physicochemical properties and computational descriptors of the screened compounds.

Comp.	Physicochemical Properties				Pharmacokinetic Properties			Drug-likeness	Lipophilicity	Solubility
	M.wt	TPSA	HBA	HBD	GI absorption	Log Kp	BBB	Druglike score	MolLogP	MolLogS (mg/L)
1	486.62	146.1	4	4	Low	-6.04	2.05	-1.27	6.55	0.17
2	518.61	202.2	6	6	Low	-6.74	1.50	-1.05	6.94	0.31
3	518.61	202.2	6	6	Low	-6.74	1.17	-0.74	5.42	1.41
4	568.73	161.74	4	4	Low	-4.87	1.03	-0.98	9.26	0.05
5	550.61	242.66	8	8	Low	-7.44	1.08	-0.64	5.91	0.74
6	587.67	220.66	8	6	Low	-7.15	1.00	-0.77	6.40	0.79
7	587.67	220.66	8	6	Low	-7.15	1.00	-0.75	7.10	0.69
8	587.67	220.66	8	6	Low	-7.15	1.00	-0.71	6.59	0.66
9	606.72	220.66	8	6	Low	-6.8	0.93	-0.40	7.59	0.72
10	638.72	239.12	10	6	Low	-7.55	0.87	-0.61	4.62	28.80
Rule	≤500	<140	<10	<5	-	-(3-5)	0-6	-	<5	-

 doi:10.20944/preprints202405.0380.v1

4. Conclusions

The paper presents the preparation of novel thiosemicarbazones, including Schiff bases, with satisfactory yields ranging from 55% to 87%. The products underwent various characterization methods including UV–Vis, FT-IR, ^{1}H NMR, ^{13}C NMR, elemental analyses, and TGA-DSC analyses. The results of our inhibition study aligned perfectly with the findings from the molecular docking analysis of these compounds against the urease enzyme. Compound **4** exhibited the strongest inhibition activity against the enzyme, while compounds **6** and **10** also demonstrated significant inhibition. Furthermore, the results for compounds **2**, **3**, **5**, and **9** exhibited a remarkable similarity. This similarity was also observed when comparing the results of the molecular docking for these compounds. Based on the molecular docking results, it can be inferred that these compounds have the ability to hinder the effectiveness of urease by interacting with the enzyme. In addition, when compared to thiourea, which is considered the reference inhibitor for this enzyme, compounds **4**, **6**, and **10** showed higher results. On the other hand, compounds **2**, **3**, **5**, and **9** exhibited nearly identical inhibition values to the inhibitor. Pharmacokinetic properties of compound **1** and compound **4** fall within the acceptable range according to major rules. Additionally, compound **10** exhibits the highest solubility among all tested compounds and falls within the acceptable lipophilicity range. Molecules shattered many of the established boundaries. Nevertheless, some of the findings from the ADMET investigation suggest that substances that show promise in inhibiting the tested enzyme in laboratory tests could be explored as potential drugs for treating various conditions caused by excessive urease activity.

Supplementary Materials: The following supporting information can be downloaded at the website of this paper posted on Preprints.org. Figure S1: IR spectrum of compound **1**. Figure S2: IR spectrum of compound **2**. Figure S3: IR spectrum of compound **3**. Figure S4: IR spectrum of compound **5**. Figure S5: IR spectrum of compound **6**. Figure S6: IR spectrum of compound **7**. Figure S7: IR spectrum of compound **8**. Figure S8: IR spectrum of compound **9**. Figure S9: IR spectrum of compound **10**. Figure S10: ^{1}H NMR spectrum of compound **1**. Figure S11: ^{1}H NMR spectrum of compound **2**. Figure S12: ^{1}H NMR spectrum of compound **3**. Figure S13: ^{1}H NMR spectrum of compound **5**. Figure S14: ^{1}H NMR spectrum of compound **6**. Figure S15: ^{1}H NMR spectrum of compound **7**. Figure S16: ^{1}H NMR spectrum of compound **8**. Figure S17: ^{1}H NMR spectrum of compound **9**. Figure S18: ^{1}H NMR spectrum of compound **10**. Figure S19: ^{13}C NMR spectrum of compound **1**. Figure S20: ^{13}C NMR spectrum of compound **2**. Figure S2: ^{13}C NMR spectrum of compound **3**. Figure S22: ^{13}C NMR spectrum of compound **5**. Figure S23: ^{13}C NMR spectrum of compound **6**. Figure S24: ^{13}C NMR spectrum of compound **7**. Figure S25: ^{13}C NMR spectrum of compound **8**. Figure S26: ^{13}C NMR spectrum of compound **9**. Figure S27: ^{13}C NMR spectrum of compound **10**. Figure S28: UV-Vis spectrum of compound **1** in DMSO. Figure S29: UV-Vis spectrum of compound **2** in DMSO. Figure S30: UV-Vis spectrum of compound **3** in DMSO. Figure S31: UV-Vis spectrum of compound **5** in DMSO. Figure S32: UV-Vis spectrum of compound **6** in DMSO. Figure S33: UV-Vis spectrum of compound **7** in DMSO. Figure S34: UV-Vis spectrum of compound **8** in DMSO. Figure S35: UV-Vis spectrum of compound **9** in DMSO. Figure S36: UV-Vis spectrum of compound **10** in DMSO. Figure S37: TGA and DSC curves for synthesized compound **1**. Figure S38: TGA and DSC curves for synthesized compound **2**. Figure S39: TGA and DSC curves for synthesized compound **3**. Figure S40: TGA and DSC curves for synthesized compound **5**. Figure S41: TGA and DSC curves for synthesized compound **6**. Figure S42: TGA and DSC curves for synthesized compound **7**. Figure S43: TGA and DSC curves for synthesized compound **8**. Figure S44: TGA and DSC curves for synthesized compound **9**. Figure S45: TGA and DSC curves for synthesized compound **10**.

Funding: This research received no external funding.

Institutional Review Board Statement: Not applicable.

Informed Consent Statement: Not applicable.

Data Availability Statement: Data are contained within the article.

Conflicts of Interest: The author declares no conflict of interest.

References

1. Da Silva, C.M.; Da Silva, D.L.; Modolo, L. V.; Alves, R.B.; De Resende, M.A.; Martins, C.V.B.; De Fátima, Â. Schiff Bases: A Short Review of Their Antimicrobial Activities. *Journal of Advanced Research* **2011**, *2*, 1–8, doi:10.1016/j.jare.2010.05.004.
2. Abou-Melha, K.S.; Faruk, H. Bimetallic Complexes of Schiff Base Bis-[4-Hydroxycuomarin-3-Yl]- 1N,5N-Thiocarbohydrazone as a Potentially Dibasic Pentadentate Ligand. Synthesis, Spectral, and Antimicrobial Properties. *Journal of the Iranian Chemical Society* **2008**, *5*, 122–134, doi:10.1007/BF03245825.
3. Ahamad, I.; Prasad, R.; Quraishi, M.A. Experimental and Quantum Chemical Characterization of the Adsorption of Some Schiff Base Compounds of Phthaloyl Thiocarbohydrazide on the Mild Steel in Acid Solutions. *Materials Chemistry and Physics* **2010**, *124*, 1155–1165, doi:10.1016/j.matchemphys.2010.08.051.
4. Aly, A.A.; Abdallah, E.M.; Ahmed, S.A.; Awad, M.K.; Rabee, M.M.; Mostafa, S.M.; Bräse, S. Metal Complexes of New Thiocarbohydrazones of Cu(I), Co(II), and Ni(II); Identification by NMR, IR, Mass, UV Spectra, and DFT Calculations. *Journal of Sulfur Chemistry* **2023**, *44*, 282–303, doi:10.1080/17415993.2022.2145846.
5. EL-Mahdy, K.M.; El-Kazak, A.M.; Abdel-Megid, M.; Seada, M.; Farouk, O. Synthesis, Characterization and Antimicrobial Activities of Some New Heterocyclic Schiff Bases Derived from Thiocarbohydrazide. *Acta Chimica Slovenica* **2016**, *63*, 18–25, doi:10.17344/acsi.2015.1555.
6. Gupta, A.K.; Prachand, S. Thiol Derivatives and Antifungal Activity. *International Journal of Pharmacy & Life Sciences* **2012**, *3*, 1848–1857.
7. Hameed, A.; al-Rashida, M.; Uroos, M.; Abid Ali, S.; Khan, K.M. Schiff Bases in Medicinal Chemistry: A Patent Review (2010-2015). *Expert Opinion on Therapeutic Patents* **2017**, *27*, 63–79, doi:10.1080/13543776.2017.1252752.
8. Kajal, A.; Bala, S.; Kamboj, S.; Sharma, N.; Saini, V. Schiff Bases: A Versatile Pharmacophore. *Journal of Catalysts* **2013**, *2013*, 1–14, doi:10.1155/2013/893512.
9. Kalem, E.; Ağar, E. Schiff Bazlarinin Biyolojik Aktivitesi Biological Activity of Schiff Bases Öz : Abstract : **2021**, *8*, 57–76.
10. Khan, S.A.; Kumar, P.; Joshi, R.; Iqbal, P.F.; Saleem, K. Synthesis and in Vitro Antibacterial Activity of New Steroidal Thiosemicarbazone Derivatives. *European Journal of Medicinal Chemistry* **2008**, *43*, 2029–2034, doi:10.1016/j.ejmech.2007.12.004.
11. Manjunatha, M.; Naik, V.H.; Kulkarni, A.D. Activities , and Spectroscopic Studies of Co (II), Ni (II), and Cu (II) Complexes of Biologically Potential Coumarin Schiff Bases. **2011**, *64*, 4264–4275.
12. Rana, K.; Pandurangan, A.; Singh, N.; Tiwari, A.K. A Systemic Review of Schiff Bases as an Analgesic, Anti-Inflammatory. *Academic Sciences* **2012**, *4*, 5–11.
13. Sathisha, M.P.; Revankar, V.K.; Pai, K.S.R. Synthesis, Structure, Electrochemistry, and Spectral Characterization of Bis-Isatin Thiocarbohydrazone Metal Complexes and Their Antitumor Activity against Ehrlich Ascites Carcinoma in Swiss Albino Mice. *Metal-Based Drugs* **2008**, *2008*, doi:10.1155/2008/362105.
14. Tribak, Z.; Chda, A.; Skalli, M.K.; Haoudi, A.; Rodi, Y.K.; Senhaji, O.; Essassi, E.M.; Cheikh, R. Ben; EL Abida, K. Theoretical Approach Using DFT and Muscle Relaxant Effects of 5-Chloroisatin Derivatives. *International Journal of Chemistry and Technology* **2018**, *2*, 105–115, doi:10.32571/ijct.446539.
15. Tuli, H.S.; Rani, A.; Kumar, M.; Khare, R. Schiff Bases as an Antimicrobial Agent: A Review Anti-Neoplastic Effects of Garcinol View Project Schiff Bases as an Antimicrobial Agent: A Review. *Journal of Biological and Chemical Sciences* **2015**, *2*, 62–91.
16. Utreja, D.; Vibha, B.S.P.; Singh, S.; Kaur, M. Schiff Bases and Their Metal Complexes as Anti-Cancer Agents: A Review. *Current Bioactive Compounds* **2015**, *11*, 215–230, doi:10.2174/1573407212666151214221219.
17. Mathew, B.; Suresh, J.; Anbazhagan, S. Synthesis, in Silico Preclinical Evaluation, Antidepressant Potential of 5-Substituted Phenyl-3-(Thiophen-2-Yl)-4,5-Dihydro-1h-Pyrazole-1-Carboxamides. *Biomedicine and Aging Pathology* **2014**, *4*, 327–333, doi:10.1016/j.biomag.2014.08.002.
18. Çavuş, M.S.; Yakan, H.; Özorak, C.; Muğlu, H.; Bakır, T.K. New N,N′-Bis(Thioamido)Thiocarbohydrazones and Carbohydrazones: Synthesis, Structure Characterization, Antioxidant Activity, Corrosion Inhibitors and DFT Studies. *Research on Chemical Intermediates* **2022**, *48*, 1593–1613, doi:10.1007/s11164-022-04659-z.
19. Shen, X.; Zhang, Z.; Cheng, C.; Liu, C.; Ma, N.; Sun, D.; Li, D.; Wang, C. Bone Regeneration and Antibacterial Properties of Calcium-Phosphorus Coatings Induced by Gentamicin-Loaded Polydopamine on Magnesium Alloys. *Biomedical Technology* **2024**, *5*, 87–101, doi:10.1016/j.bmt.2023.06.002.
20. Abu-Hussen, A.A.A.; Emara, A.A.A. Metal Complexes of Some Thiocarbohydrazone Ligands: Synthesis

and Structure. *Journal of Coordination Chemistry* **2004**, *57*, 973–987, doi:10.1080/00958970412331272412.

21. Blumenkopf, T.A.; Harrington, J.A.; Koble, C.S.; Bankston, D.D.; Morrison, R.W.; Bigham, E.C.; Styles, V.L.; Spector, T. 2-Acetylpyridine Thiocarbonohydrazones. Potent Inactivators of Herpes Simplex Virus Ribonucleotide Reductase. *Journal of Medicinal Chemistry* **1992**, *35*, 2306–2314, doi:10.1021/jm00090a022.
22. Bonaccorso, C.; Marzo, T.; La Mendola, D. Biological Applications of Thiocarbohydrazones and Their Metal Complexes: A Perspective Review. *Pharmaceuticals* **2020**, *13*, doi:10.3390/ph13010004.
23. Mosa, A.I.; Emara, A.A.A.; Yousef, J.M.; Saddiq, A.A. Novel Transition Metal Complexes of 4-Hydroxy-Coumarin-3- Thiocarbohydrazone: Pharmacodynamic of Co(III) on Rats and Antimicrobial Activity. *Spectrochimica Acta - Part A: Molecular and Biomolecular Spectroscopy* **2011**, *81*, 35–43, doi:10.1016/j.saa.2011.05.035.
24. Ebrahim Tehrani, K.H.M.; Kobarfard, F.; Azerang, P.; Mehravar, M.; Soleimani, Z.; Ghavami, G.; Sardari, S. Synthesis and Antimycobacterial Activity of Symmetric Thiocarbohydrazone Derivatives against Mycobacterium Bovis BCG. *Iranian Journal of Pharmaceutical Research* **2013**, *12*, 331–346.
25. Jarrahpour, A.; Sheikh, J.; Mounsi, I. El; Juneja, H.; Hadda, T. Ben Computational Evaluation and Experimental in Vitro Antibacterial, Antifungal and Antiviral Activity of Bis-Schiff Bases of Isatin and Its Derivatives. *Medicinal Chemistry Research* **2013**, *22*, 1203–1211, doi:10.1007/s00044-012-0127-6.
26. Papadakis, M.; Barrozo, A.; Delmotte, L.; Straistari, T.; Shova, S.; Réglier, M.; Krewald, V.; Bertaina, S.; Hardré, R.; Orio, M. How Metal Nuclearity Impacts Electrocatalytic H2 Production in Thiocarbohydrazone-Based Complexes. *Inorganics* **2023**, *11*, 1–19, doi:10.3390/inorganics11040149.
27. Cvijetić, I.N.; Herlah, B.; Marinković, A.; Perdih, A.; Bjelogrlić, S.K. Phenotypic Discovery of Thiocarbohydrazone with Anticancer Properties and Catalytic Inhibition of Human DNA Topoisomerase IIα. *Pharmaceuticals* **2023**, *16*, 341, doi:10.3390/ph16030341.
28. Ibrahim, A.A.; Kareem, M.M.; Al-Noor, T.H.; Al-Muhimeed, T.; Alobaid, A.A.; Albukhaty, S.; Sulaiman, G.M.; Jabir, M.; Taqi, Z.J.; Sahib, U.I. Pt(Ii)-Thiocarbohydrazone Complex as Cytotoxic Agent and Apoptosis Inducer in Caov-3 and Ht-29 Cells through the P53 and Caspase-8 Pathways. *Pharmaceuticals* **2021**, *14*, doi:10.3390/ph14060509.
29. Shebl, M.; Khalil, S.M.E.; Al-Gohani, F.S. Preparation, Spectral Characterization and Antimicrobial Activity of Binary and Ternary Fe(III), Co(II), Ni(II), Cu(II), Zn(II), Ce(III) and UO 2(VI) Complexes of a Thiocarbohydrazone Ligand. *Journal of Molecular Structure* **2010**, *980*, 78–87, doi:10.1016/j.molstruc.2010.06.040.
30. Cândido-Bacani, P. de M.; Reis, M.B. dos; Serpeloni, J.M.; Calvo, T.R.; Vilegas, W.; Varanda, E.A.; Cólus, I.M. de S. Mutagenicity and Genotoxicity of Isatin in Mammalian Cells in Vivo. *Mutation Research - Genetic Toxicology and Environmental Mutagenesis* **2011**, *719*, 47–51, doi:10.1016/j.mrgentox.2010.11.006.
31. Bonaccorso, C.; Grasso, G.; Musso, N.; Barresi, V.; Condorelli, D.F.; La Mendola, D.; Rizzarelli, E. Water Soluble Glucose Derivative of Thiocarbohydrazone Acts as Ionophore with Cytotoxic Effects on Tumor Cells. *Journal of Inorganic Biochemistry* **2018**, *182*, 92–102, doi:10.1016/j.jinorgbio.2018.01.019.
32. Gabr, M.T.; El-Gohary, N.S.; El-Bendary, E.R.; El-Kerdawy, M.M.; Ni, N. Isatin-β-Thiocarbohydrazones: Microwave-Assisted Synthesis, Antitumor Activity and Structure-Activity Relationship. *European Journal of Medicinal Chemistry* **2017**, *128*, 36–44, doi:10.1016/j.ejmech.2017.01.030.
33. Mousavi, S.N.; Bahrami, A.; Sadri, M.; Alipour, A. Optimization of an Ecofriendly Coating Containing Chitosan and Gelatin as Corrosion Inhibitor of Carbon Steel Grade E by Response Surface Method. *Journal of Particle Science & Technology* **2019**, *5*, 23–31, doi:10.22104/JPST.2019.3193.1136.
34. Yakan, H.; Koçyiğit, Ü.M.; Muğlu, H.; Ergul, M.; Erkan, S.; Güzel, E.; Taslimi, P.; Gülçin, İ. Potential Thiosemicarbazone-Based Enzyme Inhibitors: Assessment of Antiproliferative Activity, Metabolic Enzyme Inhibition Properties, and Molecular Docking Calculations. *Journal of Biochemical and Molecular Toxicology* **2022**, *36*, doi:10.1002/jbt.23018.
35. Aruoma, O.I.; Kaur, H.; Halliwell, B. Oxygen Free Radicals and Human Diseases. *Journal of the Royal Society of Health* **1991**, *111*, 172–177, doi:10.1177/146642409111100506.
36. Mohammed, Z.H.; Ibraheem, R.M. Anti-Oxidant Activity of Methanol Extracts of Arum Maculatum L. and Physalis Peruviana L. Plants. *Ibn Al-Haitham J. for Pure & Appl. Sci.* **2015**, *28*, 1–7.
37. Knothe, G. Some Aspects of Biodiesel Oxidative Stability ☆. **2007**, *88*, 669–677, doi:10.1016/j.fuproc.2007.01.005.
38. Di Meo, F.; Lemaur, V.; Cornil, J.; Lazzaroni, R.; Duroux, J.L.; Olivier, Y.; Trouillas, P. Free Radical Scavenging by Natural Polyphenols: Atom versus Electron Transfer. *Journal of Physical Chemistry A* **2013**,

117, 2082–2092, doi:10.1021/jp3116319.

39. Marković, Z.; Đorović, J.; Petrović, Z.D.; Petrović, V.P.; Simijonović, D. Investigation of the Antioxidant and Radical Scavenging Activities of Some Phenolic Schiff Bases with Different Free Radicals. *Journal of Molecular Modeling* **2015**, *21*, doi:10.1007/s00894-015-2840-9.
40. Saur, I.M.L.; Panstruga, R.; Schulze-Lefert, P. NOD-like Receptor-Mediated Plant Immunity: From Structure to Cell Death. *Nature Reviews Immunology* **2021**, *21*, 305–318, doi:10.1038/s41577-020-00473-z.
41. BIOVIA, D.S. No Title 2017, 779.
42. Zhang, L.; Mulrooney, S.B.; Leung, A.F.K.; Zeng, Y.; Ko, B.B.C.; Hausinger, R.P.; Sun, H. Inhibition of Urease by Bismuth(III): Implications for the Mechanism of Action of Bismuth Drugs. *BioMetals* **2006**, *19*, 503–511, doi:10.1007/s10534-005-5449-0.
43. Yenigun, S.; Ipek, Y.; Marah, S.; Demirtas, I.; Ozen, T. DNA Protection, Molecular Docking, Antioxidant, Antibacterial, Enzyme Inhibition, and Enzyme Kinetic Studies for Parietin, Isolated from Xanthoria Parietina (L.) Th. Fr. *Journal of Biomolecular Structure and Dynamics* **2024**, *42*, 848–862, doi:10.1080/07391102.2023.2196693.
44. Muğlu, H.; Yakan, H.; Misbah, A.G.A.; Çavuş, M.S.; Bakır, T.K. Synthesis, Structure Characterization and Quantum Chemical Study on Relationship between Structure and Antioxidant Properties of Novel Schiff Bases Bearing (Thio)/Carbohydrazones. *Research on Chemical Intermediates* **2021**, *47*, 4985–5005, doi:10.1007/s11164-021-04576-7.
45. Yakan, H. Preparation, Structure Elucidation, and Antioxidant Activity of New Bis(Thiosemicarbazone) Derivatives. *Turkish Journal of Chemistry* **2020**, *44*, 1085–1099, doi:10.3906/KIM-2002-76.
46. Harald Küppers *DuMonts Farben-Atlas. Über 5500 Farbnuancen Mit Kennzeichnung Und Mischanleitung*; DuMont Reiseverlag, Ed.; Ostfildern, 1978; ISBN 9783770110582.
47. Arjunan, V.; Mohan, S.; Subramanian, S.; Thimme Gowda, B. Synthesis, Fourier Transform Infrared and Raman Spectra, Assignments and Analysis of N-(Phenyl)- and N-(Chloro Substituted Phenyl)-2,2-Dichloroacetamides. *Spectrochimica Acta - Part A: Molecular and Biomolecular Spectroscopy* **2004**, *60*, 1141–1159, doi:10.1016/j.saa.2003.07.003.
48. Berthomieu, C.; Hienerwadel, R. Fourier Transform Infrared (FTIR) Spectroscopy. *Photosynthesis Research* **2009**, *101*, 157–170, doi:10.1007/s11120-009-9439-x.
49. Choudhary, N.; Bee, S.; Gupta, A.; Tandon, P. Comparative Vibrational Spectroscopic Studies, HOMO-LUMO and NBO Analysis of N-(Phenyl)-2,2-Dichloroacetamide, N-(2-Chloro Phenyl)-2,2-Dichloroacetamide and N-(4-Chloro Phenyl)-2,2-Dichloroacetamide Based on Density Functional Theory. *Computational and Theoretical Chemistry* **2013**, *1016*, 8–21, doi:10.1016/j.comptc.2013.04.008.
50. Fábián, B.; Kudar, V.; Csámpai, A.; Nagy, T.Z.; Sohár, P. Synthesis, IR-, NMR-, DFT and X-Ray Study of Ferrocenyl Heterocycles from Thiosemicarbazones. Part 21: Study on Ferrocenes. *Journal of Organometallic Chemistry* **2007**, *692*, 5621–5632, doi:10.1016/j.jorganchem.2007.09.017.
51. Lobana, T.S.; Sharma, R.; Bawa, G.; Khanna, S. Bonding and Structure Trends of Thiosemicarbazone Derivatives of Metals-An Overview. *Coordination Chemistry Reviews* **2009**, *253*, 977–1055, doi:10.1016/j.ccr.2008.07.004.
52. Nuwan De Silva, N.W.S.V.; Albu, T. V. A Theoretical Investigation on the Isomerism and the NMR Properties of Thiosemicarbazones. *Central European Journal of Chemistry* **2007**, *5*, 396–419, doi:10.2478/s11532-007-0012-1.
53. Srinivasan, B.R.; Raghavaiah, P.; Nadkarni, V.S. Reinvestigation of Growth of Urea Thiosemicarbazone Monohydrate Crystal. *Spectrochimica Acta - Part A: Molecular and Biomolecular Spectroscopy* **2013**, *112*, 84–89, doi:10.1016/j.saa.2013.04.026.
54. Wolinski, K.; Hinton, J.F.; Pulay, P. Efficient Implementation of the Gauge-Independent Atomic Orbital Method for NMR Chemical Shift Calculations. *Journal of the American Chemical Society* **1990**, *112*, 8251–8260, doi:10.1021/ja00179a005.
55. Barreto Bastos, A.M.; De Carvalho Alcântara, A.F.; Beraldo, H. Structural Analyses of 4-Benzoylpyridine Thiosemicarbazone Using NMR Techniques and Theoretical Calculations. *Tetrahedron* **2005**, *61*, 7045–7053, doi:10.1016/j.tet.2005.04.042.
56. Ebrahimi, H.P.; Hadi, J.S.; Alsalim, T.A.; Ghali, T.S.; Bolandnazar, Z. A Novel Series of Thiosemicarbazone Drugs: From Synthesis to Structure. *Spectrochimica Acta - Part A: Molecular and Biomolecular Spectroscopy* **2015**, *137*, 1067–1077, doi:10.1016/j.saa.2014.08.146.
57. Venkatachalam, T.K.; Pierens, G.K.; Reutens, D.C. Synthesis, NMR Structural Characterization and

Molecular Modeling of Substituted Thiosemicarbazones and Semicarbazones Using DFT Calculations to Prove the Syn/Anti Isomer Formation. *Magnetic Resonance in Chemistry* **2014**, *52*, 98–105, doi:10.1002/mrc.4041.

58. Chee, D.N.A.; Affan, M.A.; Ahmad, F.B.; Asaruddin, M.R.; Sam, N.; Salam, M.A.; Ismail, A.; Tan, S.H. Synthesis, Characterization, and Antibacterial Activity of Organotin(IV) Complexes with 2-Hydroxyacetophenone Thiocarbohydrazone. *Journal of Coordination Chemistry* **2011**, *64*, 4191–4200, doi:10.1080/00958972.2011.631532.
59. Kaya, Y.; Erçağ, A.; Kaya, S.; Katin, K.P.; Atilla, D. New Mixed-Ligand Iron(III) Complexes Containing Thiocarbohydrazones: Preparation, Characterization, and Chemical Reactivity Analysis through Theoretical Calculations. *Applied Organometallic Chemistry* **2022**, *36*, 1–12, doi:10.1002/aoc.6762.
60. Li, M.; Xu, J.; Li, R.; Wang, D.; Li, T.; Yuan, M.; Wang, J. Simple Preparation of Aminothiourea-Modified Chitosan as Corrosion Inhibitor and Heavy Metal Ion Adsorbent. *Journal of Colloid and Interface Science* **2014**, *417*, 131–136, doi:10.1016/j.jcis.2013.11.053.
61. Siddiqi, K.S.; Khan, S.; Nami, S.A.A.; El-ajaily, M.M. Polynuclear Transition Metal Complexes with Thiocarbohydrazide and Dithiocarbamates. *Spectrochimica Acta - Part A: Molecular and Biomolecular Spectroscopy* **2007**, *67*, 995–1002, doi:10.1016/j.saa.2006.09.019.